Energy Conversion and Management 276 (2023) 116559

Contents lists available at ScienceDirect

Energy Conversion and Management

journal homepage: www.elsevier.com/locate/enconman

Vortex induced vibration energy harvesting using magnetically coupled broadband circular-array piezoelectric patch: Modelling, parametric study, and experiments

Muhammad Hafizh [a], Asan G.A. Muthalif [a,*], Jamil Renno [a], M.R. Paurobally [a], Issam Bahadur [b], Hassen Ouakad [b], Mohamed Sultan Mohamed Ali [c]

[a] Department of Mechanical and Industrial Engineering, Qatar University, Qatar
[b] Mechanical & Industrial Engineering, Sultan Qaboos University, Oman
[c] School of Electrical Engineering, Universiti Teknologi Malaysia, Malaysia

ARTICLE INFO

Keywords:
Piezoelectric energy harvester
Broadband resonance
Magnetic coupling
Vortex-induced vibration
Shape optimization

ABSTRACT

Piezoelectric composites have become increasingly important in energy harvesting from vibration and, more recently, flow-induced vibration. The compatibility of piezoelectric devices has allowed tuning harvesters to the system's natural frequency to maximize the energy harvesting performance. However, the narrowband characteristic in piezoelectric composites is susceptible to efficiency losses when there are changes in the ambient surrounding. Thus, magnetic coupling introduces nonlinearity and can increase the broadband energy harvesting performance to account for slight variations. This paper proposes a piezoelectric energy harvester used in a pipe array to harvest oscillations from vortex-induced vibration. Adding a magnetic coupler introduces bandwidth enhancement characteristics that can accommodate slight changes in the freestream velocity. A computational simulation was used to compare different coupler shapes that can direct water flow toward the harvester array. The results show that an elliptical coupler works best and that a solid coupler has up to 50 % better performance than a hollow coupler. The experimental results showed that narrowband voltage output could reach up to 9 V in a pipe array. Furthermore, the broadband performance of magnetic coupling increased the bandwidth by up to 33 % in different orientations and distances.

1. Introduction

The infrastructure for pipelines nowadays is essential for industrialized sectors. Oil and gas, water, and chemical processes rely on pipes to transport active processes or mediums to different locations and can often extend over thousands of kilometers. The integrity and reliability of such processes are crucial to an entity, as leakages can harm humans and the environment. Sensors can be implemented to measure and monitor the active sections of the pipe. Smart sensor technology has increased in maturity over the last decade and can be implemented as a viable monitoring system [1]. Utilizing the internet of things and machine learning techniques for fault diagnosis can improve decision-making and optimize asset integrity [2,3]. However, powering such infrastructures requires power sources and cannot be connected to the main supply in the case of remote installations. Therefore, fixed energy density batteries are often employed but have a limited lifespan and require constant replacement. Alternatively, a fixed-power density energy source can be used to harvest the energy from the surroundings to power the smart sensors [4].

One of the best implementations of fixed-power density sources is vibration-energy harvesting which converts the kinetic energy of the surroundings into electrical energy. While there is still a visible gap in the literature, using the flow of the active processes leads to flow-induced vibration (FIV) if the energy harvester is placed inside the pipe. One of the more common and well-researched methods is through the use of vortex-induced vibration, where flow around a bluff body gives rise to periodic oscillations [5]. Maximum performance of energy harvesting from VIV is achieved under synchronization when the vortex shedding frequency is the same as the structural natural frequency [6–9]. Andrianne et al. [10] highlighted that experimental investigation

* Corresponding author.
E-mail addresses: muhammad.hafizh@qu.edu.qa (M. Hafizh), drasan@qu.edu.qa (A.G.A. Muthalif), jamil.renno@qu.edu.qa (J. Renno), mpaurobally@qu.edu.qa (M.R. Paurobally), bahdoor@squ.edu.om (I. Bahadur), houakad@squ.edu.om (H. Ouakad), sultan_ali@fke.utm.my (M. Sultan Mohamed Ali).

https://doi.org/10.1016/j.enconman.2022.116559
Received 8 September 2022; Received in revised form 9 November 2022; Accepted 6 December 2022
Available online 13 December 2022

Table 1
List of parameters and variables.

Symbol	Description	Value	Unit
D	Main cylinder bluff-body diameter	*21*	*mm*
L	Substrate beam length	*60*	*mm*
H	Main bluff-body height	*45*	*mm*
ρ_{beam}	Beam substrate density	*2770*	kg/m^3
$\rho_{cylinder}$	Cylinder bluff-body density	*7850*	kg/m^3
ρ_{piezo}	Active piezoelectric patch density	*7800*	kg/m^3
C_P	Clamp capacitance for piezoelectric transducer	–	*F*
Θ	Electromechanical coupling coefficient	–	NV^{-1}
A_{2807}	2807-*P2* piezoelectric active area	*196*	mm^2
D_m	Magnet diameter	*10*	*mm*
l_m	Magnet height	*4*	*mm*

in VIV-based harvesters is sufficient to power sensors and MEMS with a power output of μW to 15mW. Various designs have been implemented in the literature in harvesting the flow using piezoelectric composites oscillating with a beam and bluff body [11,12]. The piezoelectric material can convert vibration energy to electric energy when attached to a vibrating structure where the captured energy from the flow stream depends significantly on the local strain of the piezoelectric beam [13]. Using piezoelectric composites has been favorable in research due to the energy–density output, scalability, and practicality in various setups. The maximum energy extracted from the piezoelectric material is usually when the host structure undergoes (linear) resonance at synchronization [14–16]. However, the resonance is narrow-banded in the linear vibration range due to the structure often being lightly damped. Often, real applications of vibration frequencies occur over a random and broadband spectrum, reducing the efficiency of linear narrowband energy harvesting. Since vibration-based energy harvesters output

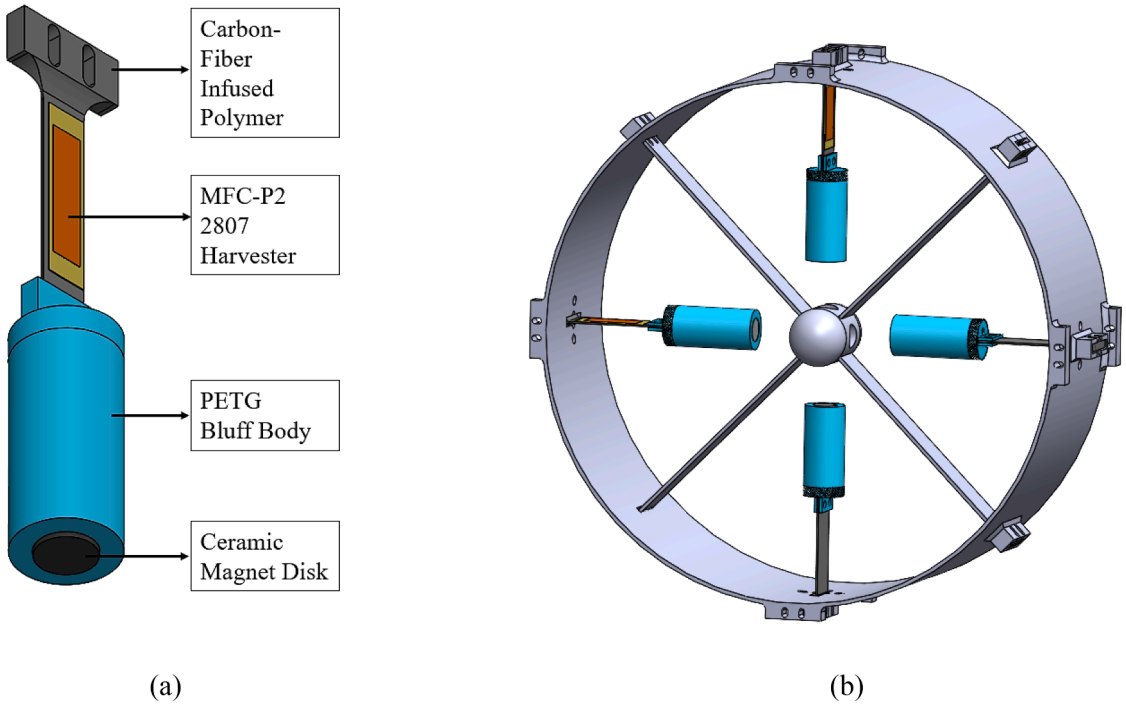

Fig. 1. Energy Harvester; (a) Material schematic; (b) Pipe assembly with coupler.

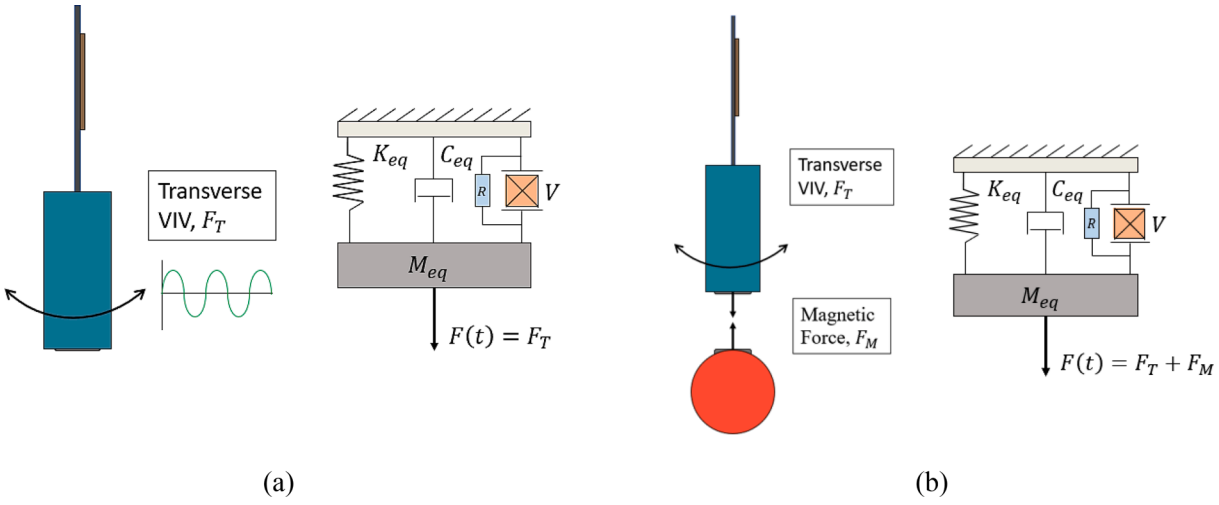

Fig. 2. Analytical model of energy harvester; (a) Standalone; (b) Magnetically coupled in repulsion.

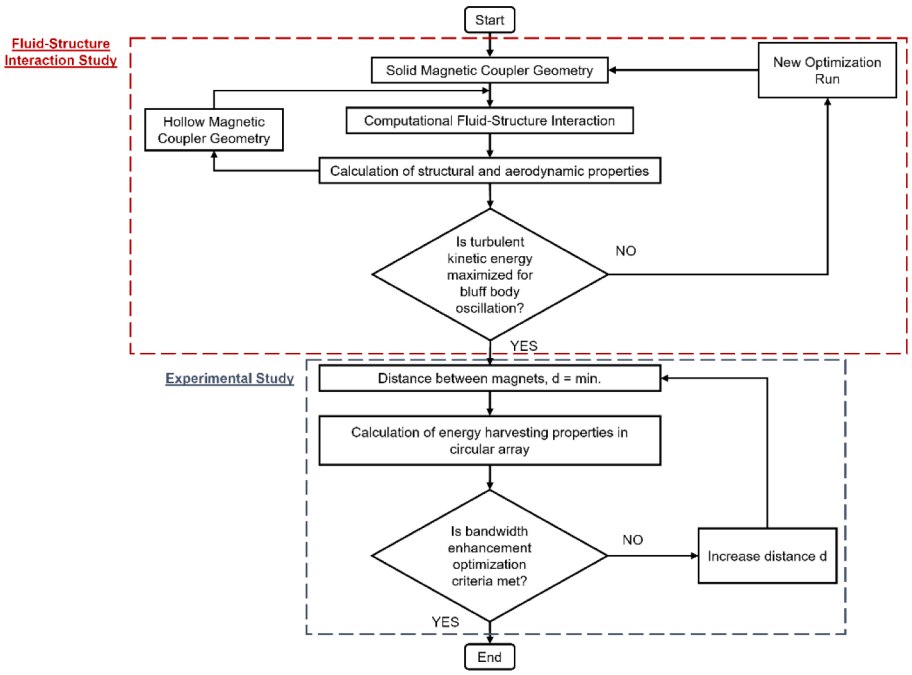

Fig. 3. Flowchart of the optimization study for circular array energy harvester.

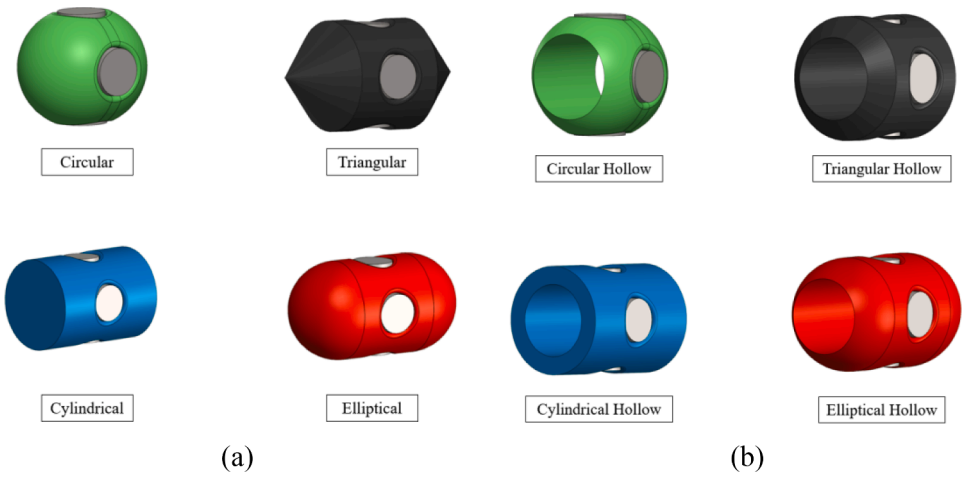

Fig. 4. Magnetic coupler shapes; (a) Solid coupler shapes; (b) Hollow coupler shapes.

maximum efficiency near the natural frequency, a slight deviation in the input source (or ambient surroundings) could drastically decrease the expected output.

To compensate for the narrowband performance of piezoelectric energy harvesters, nonlinearity can be introduced into the proposed design. One method of increasing broadband performance is adding magnetic coupling and introducing nonlinearity [17–21]. Various factors can enhance the nonlinear response, including the magnet spacing distance, flow velocity, coupled frequency, and coupled damping [22]. Nonlinear energy harvesters have demonstrated the ability to increase the frequency bandwidth [23–26]. To maximize energy harvesting, piezoelectric layers placement on a cantilever beam and the bluff body geometry should be optimally designed [27–30]. Naseer et al. [31] investigated the performance of magnetically coupled VIV-based energy harvesters for both monostable and bistable designs. Yang et al. [32] developed a magnetically coupled monostable VIV-galloping energy harvester for wind flow. Zhou et al. [33] and Qin et al. [34] demonstrated a multi-stable vortex-induced vibration-based energy harvester with permanent magnets. Zou et al. [35] developed an underwater piezoelectric energy harvester with nonlinear bistable characteristics from permanent magnets. Shan et al. [36] demonstrated numerical and experimental results of an underwater magnetic-coupled energy harvester with an output of 9.2 V.

In this paper, a nonlinear vibration-based energy harvester is developed and tuned for energy harvesting from vortex-induced vibration with bandwidth enhancement investigations using magnetic coupling and bluff body. As the infrastructure for pipes is already robust, the current work focuses on integrating an energy harvester module to work alongside existing pipelines. The work contributes to the study of energy harvesting in a pipe array for narrowband and broadband applications while tuning the shape of the coupler to increase the broadband performance. To the best of our knowledge, experimental investigative work into VIV energy harvesting with magnetic coupling in pipelines has not been adopted yet. As a result, the current work and its contribution to the gap literature focus on introducing performance enhancement with flow separation, improving the bandwidth response

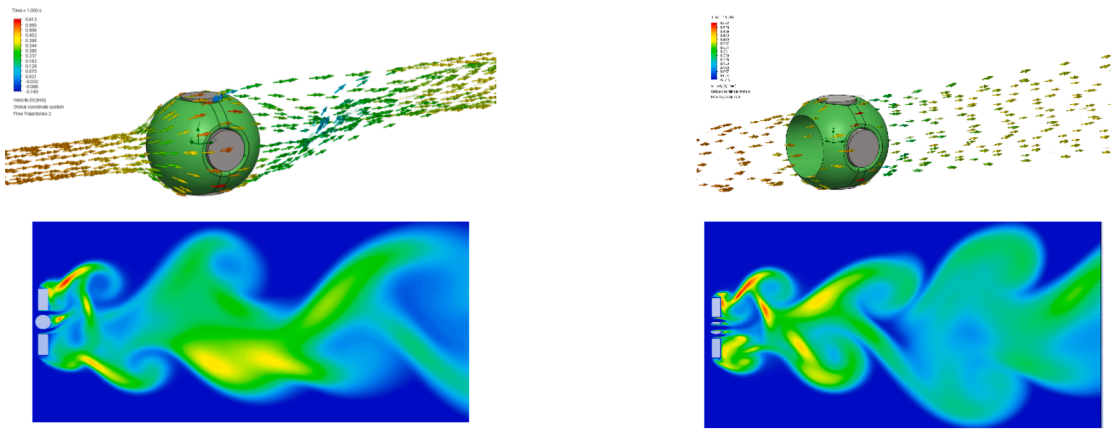

(a)

Fig. 5. Turbulent Flow Distribution in Pipe Array– left side: solid coupler, right side: hollow coupler; (a) circular; (b) triangular; (c) cylindrical; (d) elliptical.

of vortex-induced vibration energy harvesting for nonlinear applications, and optimizing magnetic separation distance within submerged fluid mediums.

In Section 2, the theoretical model of the system and structural synchronization for both a coupled and uncoupled implementation are developed. The computational domain setup is explained in Section 3. Section 4 presents the simulation study from computational fluid dynamics and experimental results of a tuned piezoelectric energy harvester submerged in a pipe array.

2. Analytical model and parameters

2.1. Analytical electromechanical model

In the proposed energy harvesting orientation, four energy harvesters were equally placed around the pipe and were equally spaced out. A macrofibre composite piezoelectric patch is attached to the beam. A bluff body is attached at the free end of the beam. The energy harvester oscillates in the direction perpendicular to the beam dictated by the vortex-induced vibrations. A ceramic magnet disk is attached to the bottom of the bluff body to allow for magnetic coupling properties in energy harvesting. The coupling of repulsive magnetic forces is attached through crossbeams and a coupler in the center. Table 1 lists the parameters and properties of the proposed energy harvester. Fig. 1 shows a close-up view of the energy harvester, the materials used in fabrication, and its arrangement around the pipe.

The bluff body oscillates perpendicular to the direction of the water flow at resonance because of vortex-induced vibration. Thus, a single degree of freedom (SDOF) model can be adopted to represent the first mode shape in this study. Fig. 2 highlights the different models used between standalone and coupled energy harvesters.

For the energy harvester with a cylindrical body and substrate beam placed underwater, vortices will form behind the bluff body such that periodic oscillations occur in the direction perpendicular to the flow of water. These oscillations modeled as a mass-spring-damper system are expressed per unit time as Eq. (1):

$$M\ddot{x} + C\dot{x} + Kx + \Theta V_p = F(t) \tag{1}$$

Where M is the equivalent mass, C is the equivalent damping, and K is the equivalent stiffness. $\ddot{x}$, $\dot{x}$ and x represents the acceleration, velocity, and displacement of the oscillations, respectively. The effect with the electromechanical piezoelectric patch is modeled with Θ as the electromechanical coupling coefficient and V_p is the voltage produced. The current that is generated from the piezoelectric macrofibre composite with term I, can be represented by Eq.2 where C^S is the clamped capacitance value [1,37]:

$$I(t) = \Theta\dot{x}(t) - C^S\dot{V}(t) \tag{2}$$

When the energy harvester is submerged in water and oscillates due to the vortices, the transverse force F_T can be modeled as a forced vibration system using a two-parameter self-excitation model with in-phase and out-of-phase forces [38] in Eq.3:

$$F_T = \frac{\rho U^2 DL(C_{mv}\sin(2\pi ft) + C_{dv}\cos(2\pi ft))}{2} \tag{3}$$

Here, ρ represents the density of the flowing fluid, U is the freestream flow velocity, D is the diameter of the bluff body and L is the wetted span of the cylinder. C_{mv} represents the oscillating inertia coefficient whilst C_{dv} represents the oscillating negative damping coefficient. The cylinder oscillating frequency is represented by f. In the case of magnetic coupling interaction, it is treated on the assumption that there is a magnetic dipole–dipole interaction between the magnets and that the magnetic dipoles were initially vertically aligned. Thus, the magnetic coupling force between two cylindrical magnets can be expressed in Eq. 4–5 [17,39]:

$$\mathrm{F_M} = \left[\frac{\beta^2 A_m^2 (l+r)^2}{\pi\tau_0 l^2}\right]\left[\frac{1}{D_0^2} + \frac{1}{(D_0+2l)^2} - \frac{2}{(D_0+l)^2}\right] \tag{4}$$

$$m = \frac{2\beta V_m}{\tau_0} \tag{5}$$

Here, τ_0 represents the permeability of the submerged fluid, D_0 is the distance between the two magnets, and β is the magnetic flux density. A_m is the cross-sectional area of the magnets, l is the height of the magnet and r is the magnet's radius. V represents the magnet volume, and m is the moment of the magnet dipoles where $m_1 = m_2$ in this case, with two repulsive cylindrical magnets.

2.2. Underwater synchronization properties

When the energy harvester is submerged underwater in the pipe array, the hydrodynamic effect of the water alters the SDOF model with added-mass parameters. This change to the equation of motion and, subsequently, the oscillation response and natural frequency of the overall harvester, as shown in Eq. (6):

$$(M + M_a)\ddot{x} + (\mathrm{C} + \mathrm{C_a} + C_p)\dot{x} + (\mathrm{K} + \mathrm{K_a} + K_p)x + \Theta V_p = F(t) \tag{6}$$

When the energy harvester is placed in a large boundary, the assumption for low damping and no added stiffness can be adopted.

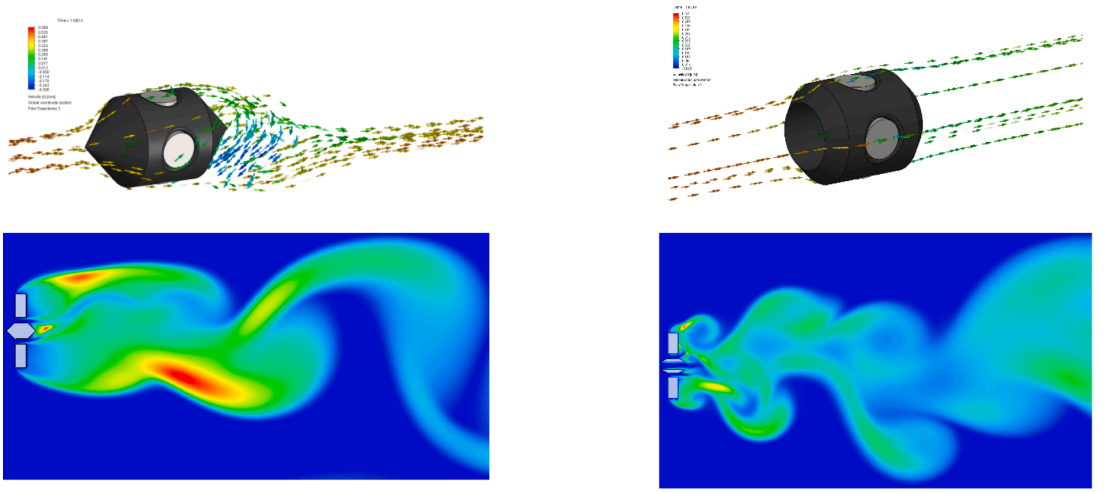

(b)

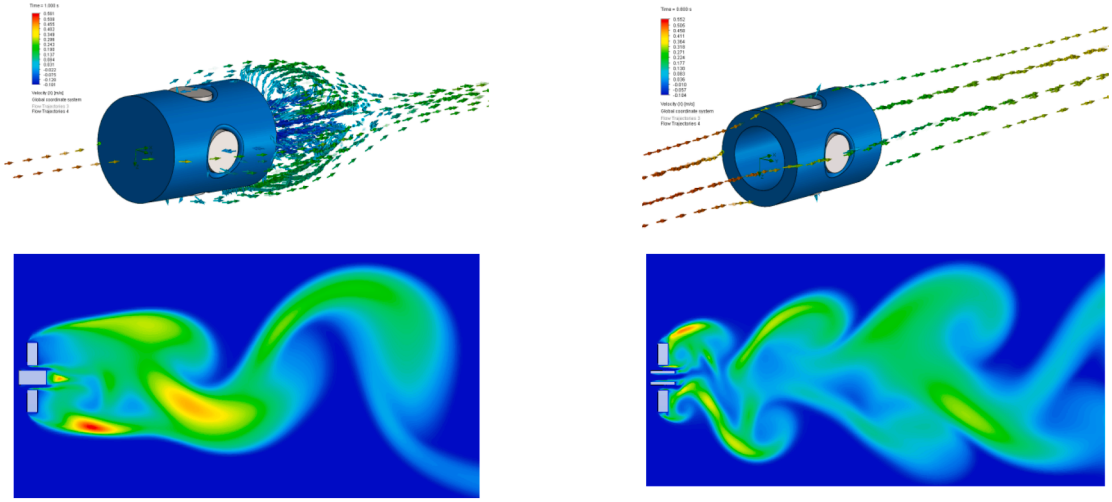

(c)

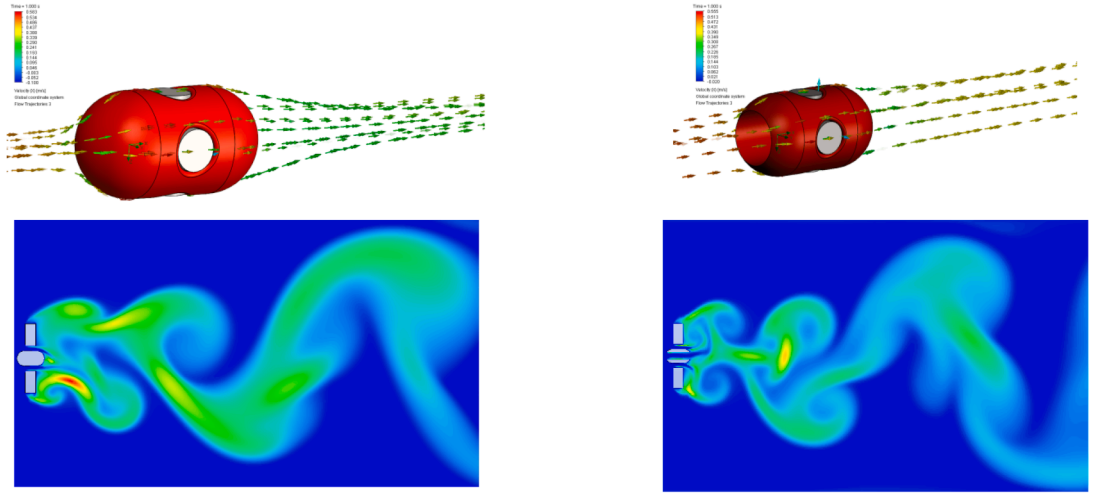

(d)

Fig. 5. (*continued*).

However, these assumptions cannot be made in a harvester array surrounded by a pipe boundary [40]. Thus, the subscript 'a' denotes added-mass properties, and 'p' is the pipe boundary interaction property. The derived ratios between air and underwater can be represented by Eq. 7–9 where the subscript 'd' represents damped, and 'w' represents underwater:

Table 2
Turbulent Kinetic Energy Simulation Comparison for Magnetic Couplers.

Configuration	Turbulent Kinetic Energy (m^2/s^2)	
	Solid Coupler	Hollow Coupler
Circular	2.30E-04	3.97E-05
Triangular	6.84E-06	6.42E-05
Cylindrical	3.86E-06	2.17E-04
Elliptical	1.69E-05	2.79E-04

$$\frac{\omega_{n,w}^2}{\omega_n^2} = \left(1+\frac{K_a}{K}\right)\left(1+\frac{M_a}{M}\right)^{-1} \tag{7}$$

$$\frac{\omega_{d,w}^2}{\omega_d^2} = \left(\frac{1-\zeta_w^2}{1-\zeta^2}\right)\left(1+\frac{K_a}{K}\right)\left(1+\frac{M_a}{M}\right)^{-1} \tag{8}$$

$$\frac{\zeta_w}{\zeta} = \left(1+\frac{C_a}{C}\right)^2\left(1+\frac{K_w}{K}\right)^{-1}\left(1+\frac{M_w}{M}\right)^{-1} \tag{9}$$

Synchronization occurs when the shedding frequency of the vortices behind the bluff body is equivalent to the structural natural frequency of the energy harvester. Therefore, tuning the energy harvester to the desired freestream velocity is important in the design process. The calculation can be approximated by using the Strouhal number that can describe the oscillating mechanism shown in Eq. (10) [41]:

$$St = \frac{f_s D}{U} \tag{10}$$

3. Setup

The computational fluid dynamics (CFD) simulation is used to simulate the flow around the bluff body and the coupler inside the pipe to determine the best configuration. The domain and setup of the CFD were based on the simulations developed by the author's previous work [12]. The simulation was modeled on ANSYS v. 2020R2 CFD software using second-order spatial discretization and implicit transient formation settings. Initialization of values was achieved with good agreement compared to similar VIV simulations in the literature and was used to verify that the solution obtained was independent of the mesh resolution. An additional mesh refinement region was defined around the bluff body and magnetic coupler shapes with inflation and sizing techniques. The computational domain has a total length of 40D and a width of 20D, where D refers to the diameter of the bluff body at 21 mm. The bluff

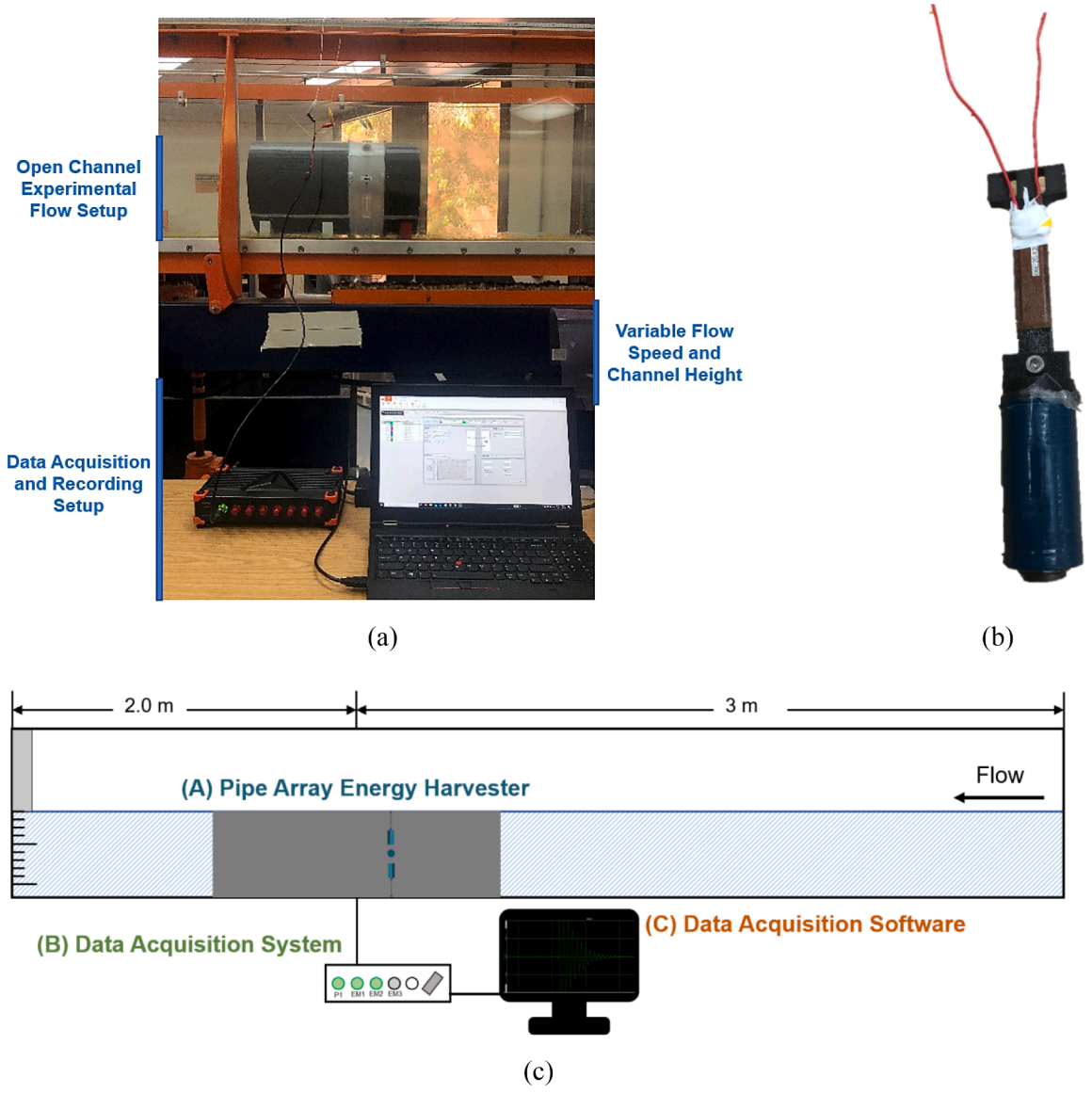

Fig. 6. Experimental setup; (a) Pipe array picture; (b) Energy harvester; (c) Schematic.

Table 3
Natural frequency of energy harvesters around the pipe array; (a) in the air; (b) submerged in water.

Top Orientation		Side Orientation		Bottom Orientation	
$\omega_{t,a}$	$\zeta_{t,a}$	$\omega_{s,a}$	$\zeta_{s,a}$	$\omega_{b,a}$	$\zeta_{b,a}$
4.5	0.10	5.0	0.075	4.2	0.13
(a)					
Top Orientation		Side Orientation		Bottom Orientation	
$\omega_{t,w}$	$\zeta_{t,w}$	$\omega_{s,w}$	$\zeta_{s,w}$	$\omega_{b,w}$	$\zeta_{b,w}$
3.9	0.18	3.6	0.14	3.3	0.20
(b)					

body and coupler have 10D upstream and 30D downstream with 10D width on both sides. Inlet velocity was applied at different Reynolds numbers near the synchronization range. The $k-\omega$ SST turbulence model was implemented using a SIMPLE Algorithm and a 2nd-order transport equation to solve the inner region of the boundary layer [42]. A no-slip boundary was applied to the top and bottom of the boundary and an average static pressure of 0 Pa was set for the outlet boundary. When meshing, the distance between the cylinder wall and the first node, y^+ was less than unity and adjusted accordingly. Finally, the time step used was 0.002 s solved over 20 s with 15 iterations per time step to show vortex shedding behavior. Once the residuals reached a satisfactory level, the simulation was converged for the pressure, turbulence, and velocity. The flowchart for the computational and experimental optimization study is shown in Fig. 3.

4. Results

4.1. Computational shape optimization

Different tip shape configurations were considered for the shape optimization study of a magnetic coupler with the main purpose of redirecting the flow towards the 4 sides of the energy harvester to maximize turbulence and voltage output. The different shapes shown consisted of solid and hollow variations of circular, triangular, cylindrical, and elliptical shapes shown in Fig. 4. The fluid–structure interaction focuses on structural and aerodynamic aspects that will be incorporated into the shape optimization of the magnetic coupler [43]. The flow-field simulation of a magnetically coupled harvester was also studied in the literature, highlighting that the addition of the coupler greatly impacts the vorticity, pressure, and velocity distribution [44]. The magnetic coupler geometries were found based on a preliminary

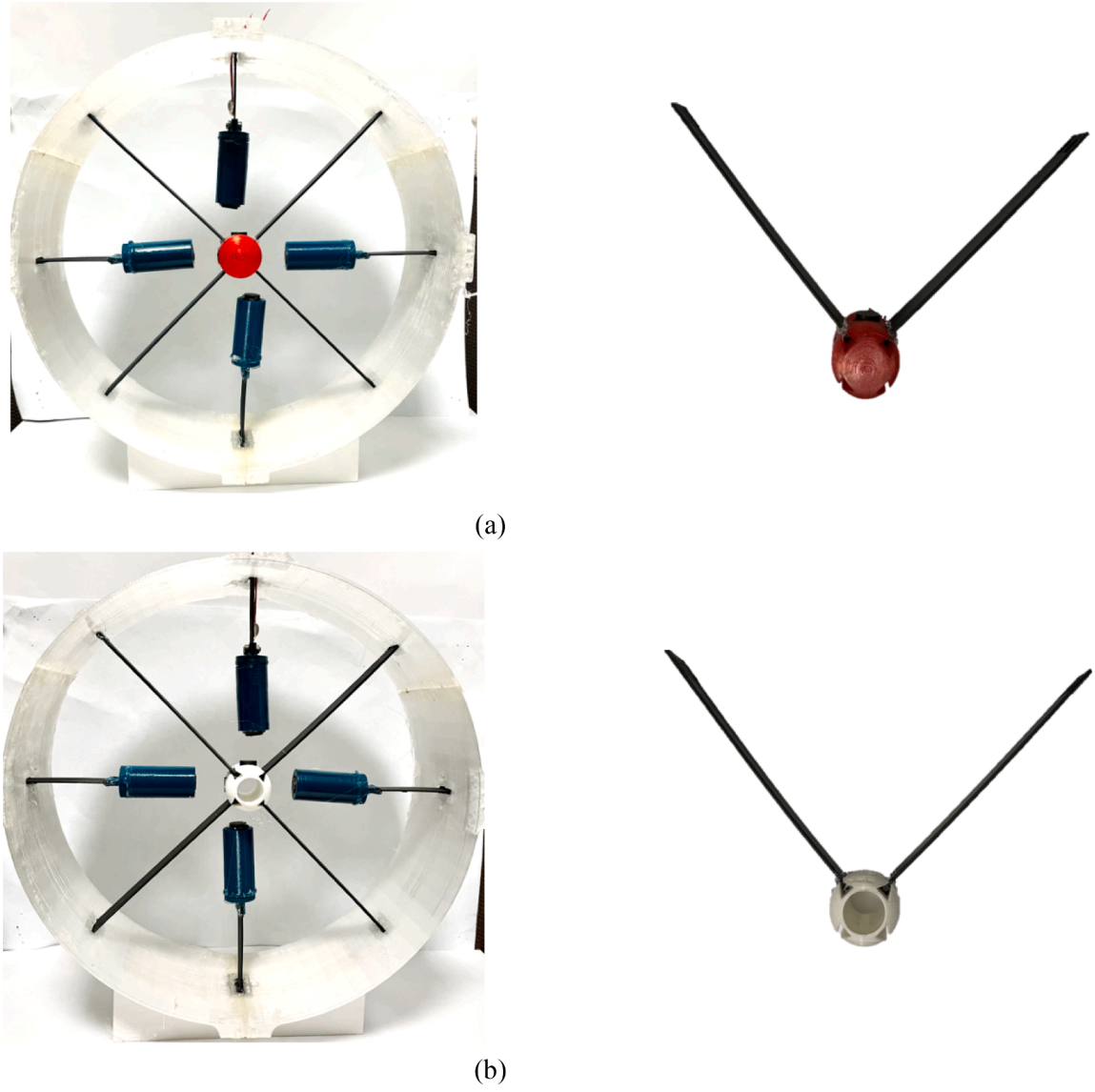

Fig. 7. Magnetically coupled energy harvester in top orientation: (a) Solid Coupler; (b) Hollow Coupler.

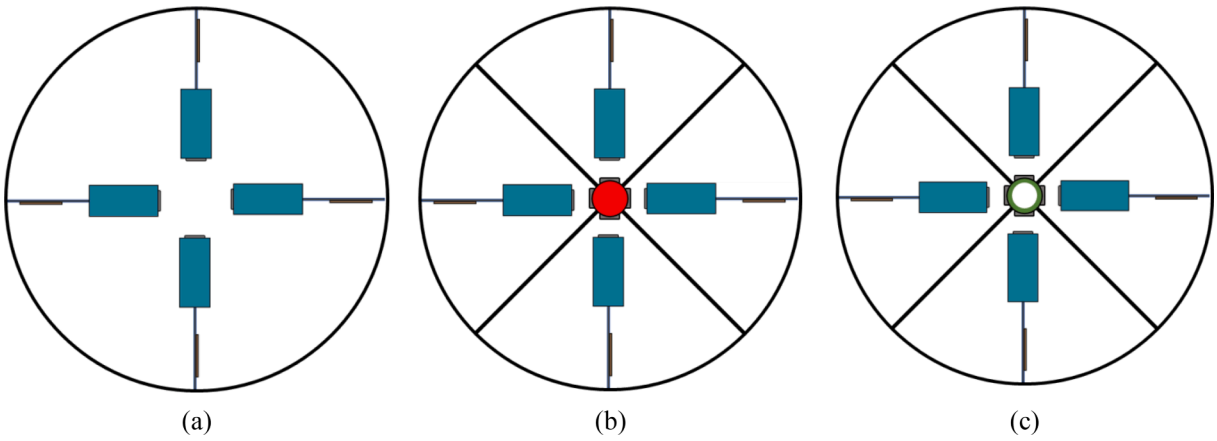

Fig. 8. Experimental Pipe Array Arrangements; (a) No Coupler; (b) Solid Coupler; (c) Hollow Coupler.

optimization study performed on coupler tip shape and distance for triangular, cylindrical, and elliptical shapes with the same geometrical properties. The circular magnetic coupler was smaller in shape and matched to the energy harvester bluff body to compare the effect of a leading-edge interaction on the flow distribution.

An external flow CFD simulation was initially run to visualize the flow distribution around each coupler shape at 0.5 m/s. In the 3D external simulation, the velocity distribution around the shape contours was compared between the different shapes. In a 2D simulation, the two energy harvester bluff bodies were added to the side of the magnetic coupler, and the interaction of fluid flow between the bodies was simulated. The results of the computational flow simulation are shown in Fig. 5.

The localized turbulent kinetic energy around the cylindrical bluff bodies was measured and shown in Table 2 taken after 10 s. The highest turbulence would be generated from sudden geometry changes, which correspond to the flat shape. Turbulent vortices formed behind the bluff body and then subsequently dissipated behind the flow. The circular magnetic coupler generated a lot of turbulence for the cylinders in the solid coupler, which could have been due to turbulence formation over a shorter distance. In the 3D model, the cylindrical configuration had turbulence formation behind the flat surface; while turbulence formation is required for vibration-based energy harvesting applications, the random and unpredictable vortex formed would not benefit a pipe arrangement because the flow cannot be directed to the 4 sides equally. Taking advantage of the solid coupler could result in more energy harvested since the distribution of flow is being redirected toward the energy harvester array around the pipe, which the elliptical shape would best achieve. The hollow coupler does not disturb the flow much and allows most of the fluid in the center to pass through undisturbed and would have a lower energy harvesting performance. The turbulence distribution is shown to form behind the coupler and cylinder bluff bodies.

After running the CFD simulations around the magnetic coupler, the results can be extended to include the energy harvesters. The simulation highlighted the differences in turbulent kinetic energy and the velocity distribution of the magnetic couplers when subjected to flow near the synchronization region. The hollow circular coupler provided the least turbulence in the flow due to its smaller size and smooth body contours. Therefore, using a cylindrical shape would not be feasible in increasing the harvesting performance and bandwidth enhancement. The triangular magnetic coupler increases the energy compared to the cylindrical shape. Still, it has less turbulence formation compared to the elliptical coupler, and the sharp tip shape adds a layer of tuning. A sudden change in the shape would direct the flow around the coupler, but the flow distribution depended on the symmetry and flow. If the fluid medium started to become turbulent before the coupler, then directing the fluid flow would no longer be uniform and would introduce additional nonlinearity. Thus, the triangular coupler shape is not feasible for the pipe array. Finally, both the cylindrical and the elliptical coupler shapes highlighted a good uniform flow around the body. However, the turbulence accumulation behind the cylindrical body is undesirable as it diminishes the directional flow towards the bluff bodies. The cylindrical coupler shape still produces the lowest turbulent kinetic energy due to its lack of flow direction when comparing hollow coupler results. However, unlike the solid coupler results, the elliptical coupler produced the highest turbulent kinetic energy for the elliptical shape. These values highlight the importance of the redirection contour from the magnetic couplers towards the bluff body when the coupler body is removed. Therefore, the best selection for the pipe array would be to use the elliptical coupler due to its gradual change in geometry that helps direct the water flow.

4.2. *Experimental verification*

An experimental setup was constructed in a water channel to verify the analytical models and simulation results. A pipe was constructed out of 3 sections and firmly seated on a holder in the water channel. The water channel had an adjustable gate and valve to control the water height and flow velocity. Compared to conventional piezoaeroelastic energy harvesters used in wind tunnels found in literature, experimental investigation with water is more complex as the insulated electronics and the solid–fluid coupling require more stringent considerations. Therefore, tuning the energy harvester to the synchronization shedding frequency has to incorporate the 'added-mass' hydrodynamic effects. In this paper, the energy harvester has been tuned to reach synchronization at the maximum flow rate. Fig. 6 shows the experimental setup with the energy harvester and data acquisition. The Dewesoft Sirius data acquisition (DAQ) device with installed DewesoftX software was used to measure the voltage output from the piezoelectric patch during the experiment. Each measurement was taken with 30 s of recording time on the DAQ after a steady flow was achieved at the system's natural frequency. A sampling frequency of 5000 Hz was used, and the time domain results were then exported into Fast Fourier transform (FFT) with a 0.1 Hz resolution with a Hanning window. The FFT analysis converted the time-domain response into an averaged graphical plot. The frequency domain analysis captured the linear peaks averaged over the entire time with an overlap average of 66.7 %; the higher overlap and windowing technique ensures that each sample in the time domain is exactly accounted for in the frequency domain to minimize missing or unequally weighted portions of the time signal [45,46].

The natural frequencies of the energy harvester in the uncoupled pipe array are shown in Table 3. A different thickness (2 layers) substrate beam was used for the top energy harvester to lower the

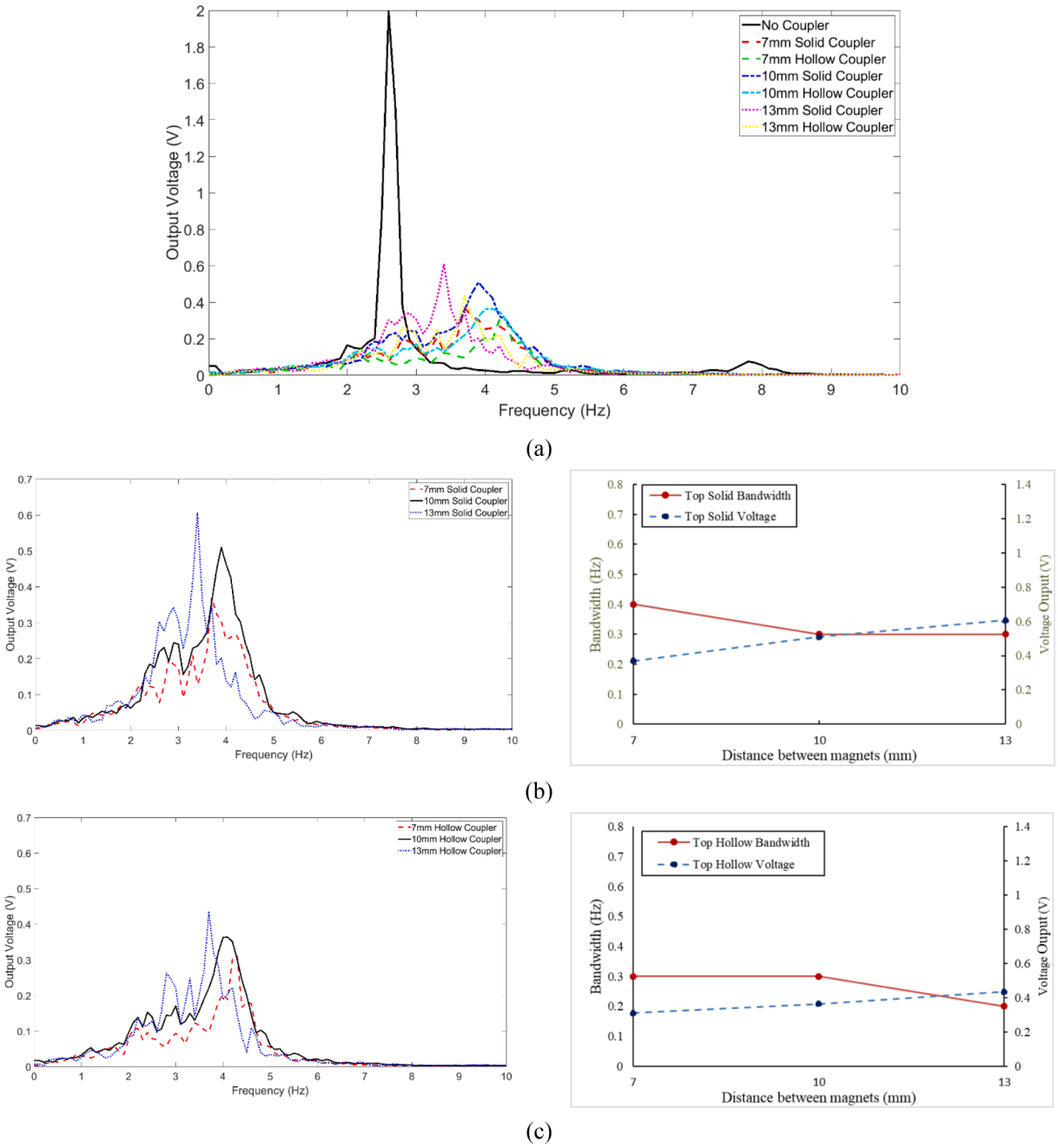

Fig. 9. Top Energy Harvester; (a) Overall harvesting performance; (b) Solid coupler; (c) Hollow coupler.

structure's natural frequency. The side and bottom energy harvester had 3 layers in the substrate beam to not deform plastically as gravity has more effect on the bluff body. With the addition of the buoyancy force from the water, the beam in the side orientation does not sag. The magnetic couplers were fixed diagonally to the pipe array, as shown in Fig. 7.

4.3. Harvesting with bandwidth enhancement

The structural natural frequency is tied to the vortex shedding frequency under synchronization. However, the air measurements differ when it is submerged in water and when it is attached inside a pipe array due to 'added' effects from water. Additionally, the introduction of a magnetic coupler that is sufficiently strong enough can increase the natural frequency of the energy harvester. Thus, tuning the beam and bluff body is required to ensure that the energy harvester can achieve maximum performance for the specified freestream flow velocity range. The different orientations of the energy harvester around the pipe array are shown in Fig. 8, where the distance from the magnetic coupler is a varied parameter. The results for the top energy harvester are shown in Fig. 9, the side energy harvester is shown in Fig. 10, and the bottom energy harvester is shown in Fig. 11. A comparison of the bandwidth enhancement and voltage output between coupled energy harvesting is highlighted in Table 4, Table 5, and Table 6 for top, side, and bottom energy harvesting orientation, respectively.

The frequency-domain plots highlight that the linear resonance of uncoupled systems still outperforms broadband energy harvesters by up to 93 % voltage output. However, the broadband property of the magnetic coupling increases the bandwidth by 33 %, provides better performance across a range of velocities and allows for improved performance using half-power bandwidth enhancement analysis. Due to the low frequency (1–7 Hz) measurement and design of the optimized

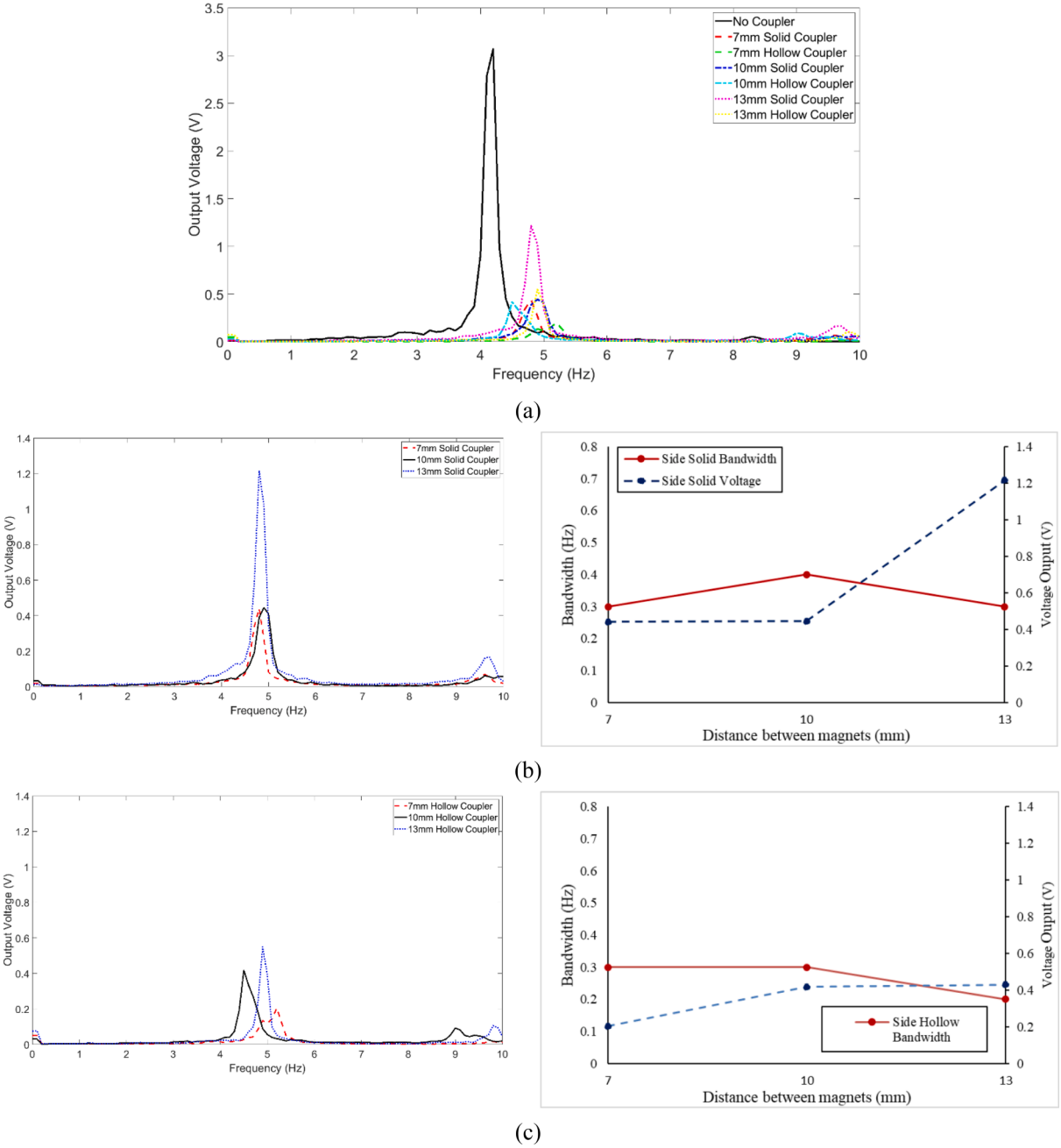

Fig. 10. Side Energy Harvester; (a) Overall harvesting performance; (b) Solid coupler; (c) Hollow coupler.

energy harvester, the performance of the bandwidth enhancement is limited by the resolution of the data acquisition. Despite this, the side energy harvester performance still provided the highest voltage output of up to 1.3 V with a 13 mm coupler distance and is the highest recorded value in all orientations. Moreover, the bottom energy harvester voltage reduction was not as severe as the other orientations and was as low as 8 % for a 10 mm solid coupler distance.

Since there are two side harvesters in the array and with the highest maximum voltage, the priority of shape optimization should go to them when designing and tuning for flow-induced vibration. The side harvesters were able to produce the highest voltage output as the gravitational acceleration helped increase the piezoelectric strain. Tuning the top energy harvester can be achieved by decreasing the system's effective stiffness so that the system's natural frequency is like the other energy harvesters in the pipe array. However, the magnetic field should be adjusted so that the top orientation is not stuck to one side due to a weaker restoring force, as this reduces the energy harvesting output and diminishes the effect of bandwidth enhancement. The bottom energy harvester presented significant damping in its oscillations but showed a better broadband performance than the top and side energy harvesters. The solid coupler also has a higher energy harvesting performance than the hollow magnetic coupler because of the water flow redirection highlighted in the CFD simulation studies.

The experimental results highlighted the effects of nonlinear magnetic coupling on the VIV-based piezoelectric energy harvester, where a selection of magnet separation distance can be optimized. By using permanent magnets in the pipe array, the increase in the distance leads to decreased magnetic force interaction and perceived lower 'equivalent stiffness'. For repulsive magnetic coupling used in this study, the critical minimum separation distance is defined when the magnetic stiffness exceeds the beam's yield strength, which prevents the harmonic oscillations from returning to its equilibrium position as the system is overly

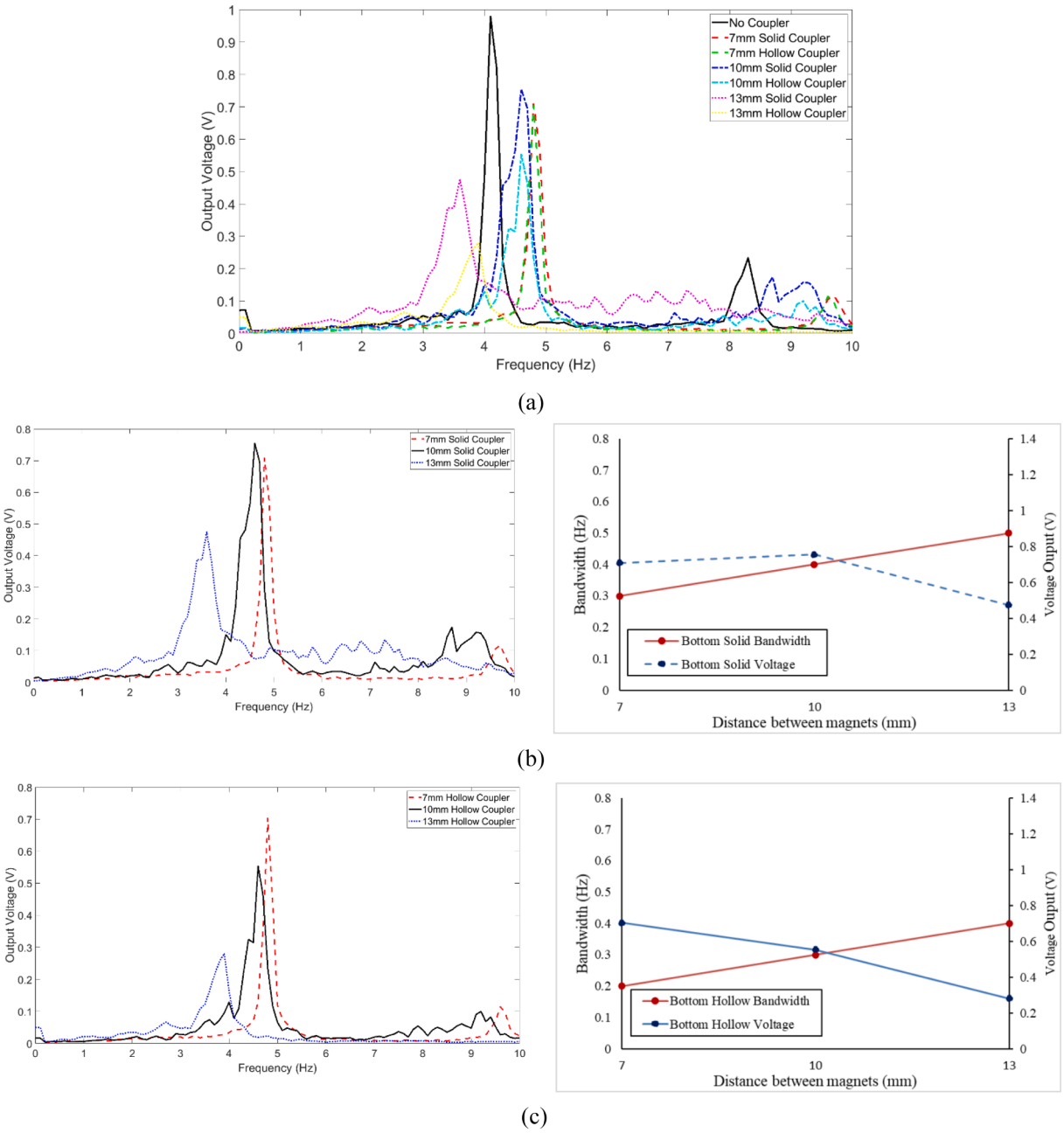

Fig. 11. Bottom Energy Harvester; (a) Overall harvesting performance; (b) Solid coupler; (c) Hollow coupler.

Table 4
Broadband Performance Comparison for Top Energy Harvester.

Broadband Performance: Top Harvester	Distance between Magnets		
	7 mm	10 mm	13 mm
Solid: Voltage Reduction	81 %	74 %	70 %
Solid: Bandwidth Enhancement	33 %	0 %	0 %
Hollow: Voltage Reduction	84 %	82 %	78 %
Hollow: Bandwidth Enhancement	0 %	0 %	–33 %

Table 5
Broadband Performance Comparison for Side Energy Harvester.

Broadband Performance Comparison: Side Harvester	Distance between Magnets		
	7 mm	10 mm	13 mm
Solid: Voltage Reduction	86 %	85 %	60 %
Solid: Bandwidth Enhancement	0 %	33 %	0 %
Hollow: Voltage Reduction	93 %	86 %	82 %
Hollow: Bandwidth Enhancement	0 %	0 %	–33 %

stiff and the beam itself buckles [47]. After taking the FFT, the bandwidth and voltage results shown for the different orientations were highlighted in the frequency domain. The results of RMS voltage output in the different orientations are shown in Fig. 12. The different distances of the magnetic coupler to the energy harvester were compared. Based on the results highlighted in the frequency and time domain, the solid magnetic coupler was the most effective in energy harvesting and redirecting flow, as shown in the CFD simulations. The top and bottom energy harvester performed best with a 10 mm coupler distance. The side energy harvester performed best with a 13 mm coupler distance to allow for sufficient oscillations so that the added stiffness does not 'lock' the bluff body with the force of gravity.

Table 6
Broadband Performance Comparison for Side Energy Harvester.

Broadband Performance: Bottom Harvester	Distance between Magnets		
	7 mm	10 mm	13 mm
Solid: Voltage Reduction	38 %	8 %	27 %
Solid: Bandwidth Enhancement	0 %	33 %	−67 %
Hollow: Voltage Reduction	28 %	44 %	71 %
Hollow: Bandwidth Enhancement	−33 %	0 %	33 %

5. Conclusions

This paper proposed a tuned vibration-based piezoelectric energy harvester with bandwidth enhancement to maximize the energy harvester from vortex-induced vibrations in the broadband range. MFC-*P2* piezoelectric patches harvested the kinetic energy from the vortices formed behind the bluff body, resulting in transverse oscillations. A theoretical model for the system's electromechanical performance and output was presented with structural synchronization due to the added mass effects in a submerged pipe array. A computational fluid analysis using $k-\omega$ SST turbulence model was used in ANSYS to visualize the

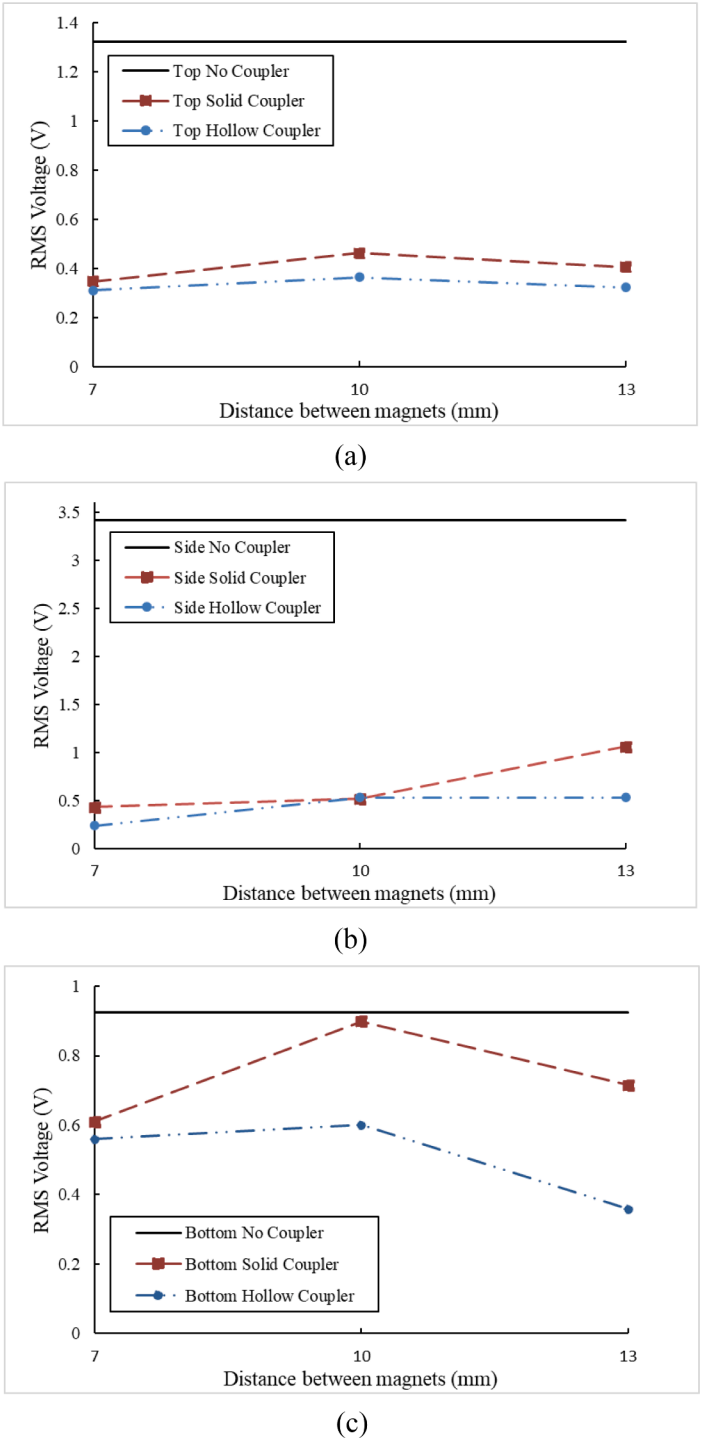

Fig. 12. Average RMS voltage output of pipe array energy harvester; (a) Top orientation; (b) Side orientation; (c) Bottom orientation.

flow behavior around different magnetic coupler shapes. An experimental validation study on the natural frequency and energy harvesting performance was conducted with the magnetic couplers. The results of this energy harvesting study highlighted:

- The elliptical magnetic coupler shape is the best flow distribution around a pipe array due to the gradual transition of its shape and the uniformity of flow redirected to the energy harvesters.
- Side energy harvesters are the priority for design and tuning to reach the maximum output voltage during synchronization. The experimental data highlighted that both side harvesters can output up to 6.2 V.
- The narrowband peak voltage output of the energy harvesters harvested up to 93 % more, but the magnetic couplers increased the frequency bandwidth response by 33 %.
- As the magnetic coupler got farther, the voltage output reduction was reduced but increased the bandwidth enhancement for the top, and side orientations. The bottom coupled orientation saw the least voltage reduction and performed best when the coupler was 10 mm away.

Magnets and nonlinear modeling provide an excellent foundation for bandwidth enhancement in frequency responses. However, a bandwidth-enhanced harvester that does not compromise on the peak performance output remains a future challenge in VIV energy harvesting. Implementing a self-aligning mechanism that can adjust for changes in the flow stream can improve efficiency with a nonlinear broadband response. Furthermore, integrating machine learning algorithms to improve the system performance analysis can be a further extension of energy harvesting applications from pipeline infrastructures.

CRediT authorship contribution statement

Muhammad Hafizh: Data curation, Investigation, Methodology, Writing – original draft, Writing – review & editing. **Asan G.A. Muthalif:** Conceptualization, Methodology, Validation, Funding acquisition, Project administration, Supervision, Visualization, Writing – review & editing. **Jamil Renno:** Methodology, Validation, Writing – review & editing. **M.R. Paurobally:** Methodology, Validation, Writing – review & editing. **Issam Bahadur:** Methodology, Resources. **Hassen Ouakad:** Methodology, Resources. **Mohamed Sultan Mohamed Ali:** Resources, Writing – review & editing.

Declaration of Competing Interest

The authors declare that they have no known competing financial interests or personal relationships that could have appeared to influence the work reported in this paper.

Data availability

Data will be made available on request.

Acknowledgements

This work was partially supported by Qatar University - International Research Collaboration Grant no. IRCC-2020-017, National Priorities Research Program Grant no. NPRP 11S – 1220 – 170112 and Student Grant no. QUST-1-CENG-2022-321. The findings achieved herein are solely the responsibility of the authors.

References

[1] Roundy S, Wright PK. A piezoelectric vibration based generator for wireless electronics. Smart Mater Struct 2004;13:1131–42. https://doi.org/10.1088/0964-1726/13/5/018.
[2] Elsisi M, Tran MQ, Mahmoud K, Mansour DEA, Lehtonen M, Darwish MMF. Effective IoT-based deep learning platform for online fault diagnosis of power transformers against cyberattacks and data uncertainties. Meas J Int Meas Confed 2022;190:110686. https://doi.org/10.1016/j.measurement.2021.110686.
[3] Tran M-Q, Elsisi M, Liu M-K, Vu VQ, Mahmoud K, Darwish MMF, et al. Reliable Deep Learning and IoT-Based Monitoring System for Secure Computer Numerical Control Machines Against Cyber-Attacks With Experimental Verification. IEEE Access 2022;10:23186–97.
[4] Dutoit NE, Wardle BL, Kim S-G. Desin considerations for MEMS-scale piezoelectric mechanical vibration energy harvesters. Integr Ferroelectr 2005;71:121–60. https://doi.org/10.1080/10584580590964574.
[5] Pobering S, Ebermeyer S, Schwesinger N. Generation of electrical energy using short piezoelectric cantilevers in flowing media. ProcSPIE 2009;7288:109–16. https://doi.org/10.1117/12.815189.
[6] Williamson CHK, Govardhan R. A brief review of recent results in vortex-induced vibrations. J Wind Eng Ind Aerodyn 2008;96:713–35. https://doi.org/10.1016/j.jweia.2007.06.019.
[7] Jia J, Shan X, Upadrashta D, Xie T, Yang Y, Song R. Modeling and Analysis of Upright Piezoelectric Energy Harvester under Aerodynamic Vortex-induced Vibration. Micromachines 2018;9:667. https://doi.org/10.3390/mi9120667.
[8] Wang J, Ran J, Zhang Z. Energy harvester based on the synchronization phenomenon of a circular cylinder. Math Probl Eng 2014;2014:1–9.
[9] Gabbai RD, Benaroya H. An overview of modeling and experiments of vortex-induced vibration of circular cylinders. J Sound Vib 2005;282:575–616. https://doi.org/10.1016/j.jsv.2004.04.017.
[10] Andrianne T, Aryoputro RP, Laurent P, Colson G, Amandolèse X, Hémon P. Energy harvesting from different aeroelastic instabilities of a square cylinder. J Wind Eng Ind Aerodyn 2018;172:164–9. https://doi.org/10.1016/j.jweia.2017.10.031.
[11] Wang J, Geng L, Ding L, Zhu H, Yurchenko D. The state-of-the-art review on energy harvesting from flow-induced vibrations. Appl Energy 2020;267:114902. https://doi.org/10.1016/j.apenergy.2020.114902.
[12] Muthalif AGA, Hafizh M, Renno J, Paurobally MR. An enhanced hybrid piezoelectric–electromagnetic energy harvester using dual-mass system for vortex-induced vibrations. JVC/Journal Vib Control 2021;27:2848–61. https://doi.org/10.1177/10775463211041875.
[13] Zheng B, Hae CC, Gea C. Topology optimization of energy harvesting devices using piezoelectric materials. Struct Multidiscip Optim 2009;38:17–23. https://doi.org/10.1007/s00158-008-0265-0.
[14] Mohamed K, Elgamal H, Kouritem SA. An experimental validation of a new shape optimization technique for piezoelectric harvesting cantilever beams. Alexandria Eng J 2021;60:1751–66. https://doi.org/10.1016/J.AEJ.2020.11.024.
[15] Muthalif AGA, Nordin NHD. Optimal piezoelectric beam shape for single and broadband vibration energy harvesting: Modeling, simulation and experimental results. Mech Syst Signal Process 2015;54:417–26. https://doi.org/10.1016/j.ymssp.2014.07.014.
[16] Karadag CV, Ertarla S, Topaloglu N, Okyar AF. Optimization of beam profiles for improved piezoelectric energy harvesting efficiency. Struct Multidiscip Optim 2021;63:631–43. https://doi.org/10.1007/s00158-020-02714-0.
[17] Ibrahim DS, Muthalif AGA, Nordin NHD, Saleh T. Comparative study of conventional and magnetically coupled piezoelectric energy harvester to optimize output voltage and bandwidth. Microsyst Technol 2017;23:2663–74. https://doi.org/10.1007/s00542-016-3066-1.
[18] Lo YC, Chen CC, Shu YC, Lumentut MF. Broadband piezoelectric energy harvesting induced by mixed resonant modes under magnetic plucking. Smart Mater Struct 2021;30(10):105026.
[19] Jiang J, Liu S, Feng L, Zhao D. A Review of Piezoelectric Vibration Energy Harvesting with Magnetic Coupling Based on Different Structural Characteristics. Micromachines 2021:12. https://doi.org/10.3390/mi12040436.
[20] Lin J-T, Lee B, Alphenaar B. The magnetic coupling of a piezoelectric cantilever for enhanced energy harvesting efficiency. Smart Mater Struct 2010;19(4):045012.
[21] Wang H, Tang L. Modeling and experiment of bistable two-degree-of-freedom energy harvester with magnetic coupling. Mech Syst Signal Process 2017;86:29–39. https://doi.org/10.1016/j.ymssp.2016.10.001.
[22] Naseer R, Dai H, Abdelkefi A, Wang L. Comparative study of piezoelectric vortex-induced vibration-based energy harvesters with multi-stability characteristics. Energies 2019:13. https://doi.org/10.3390/en13010071.
[23] Ibrahima DS, Muthalif AGA, Saleh T. A Piezoelectric Based Energy Harvester with Magnetic Interactions: Modelling and Simulation. Adv Mater Res 2015;1115:549–54. https://doi.org/10.4028/WWW.SCIENTIFIC.NET/AMR.1115.549.
[24] Wen S, Wu Z, Xu Q. Design of a Novel Two-Directional Piezoelectric Energy Harvester with Permanent Magnets and Multistage Force Amplifier. IEEE Trans Ultrason Ferroelectr Freq Control 2020;67:840–9. https://doi.org/10.1109/TUFFC.2019.2956773.
[25] Lumentut MF, Francis LA, Howard IM. Analytical techniques for broadband multielectromechanical piezoelectric bimorph beams with multifrequency power harvesting. IEEE Trans Ultrason Ferroelectr Freq Control 2012;59:2555–68. https://doi.org/10.1109/TUFFC.2012.2489.
[26] Staaf LGH, Smith AD, Lundgren P, Folkow PD, Enoksson P. Effective piezoelectric energy harvesting with bandwidth enhancement by assymetry augmented self-tuning of conjoined cantilevers. Int J Mech Sci 2019;150:1–11. https://doi.org/10.1016/J.IJMECSCI.2018.09.050.
[27] Akaydin HD, Elvin N, Andreopoulos Y. The performance of a self-excited fluidic energy harvester. Smart Mater Struct 2012;21(2):025007.
[28] Zhang LB, Dai HL, Abdelkefi A, Wang L. Experimental investigation of aerodynamic energy harvester with different interference cylinder cross-sections. Energy 2019;167:970–81. https://doi.org/10.1016/j.energy.2018.11.059.

[29] Hafizh M, Muthalif AGA, Renno J, Paurobally MR, Arab MA, Bahadur I, et al. A hybrid piezoelectric-electromagnetic nonlinear vibration energy harvester excited by fluid flow. Comptes Rendus Mécanique 2021;349:65–81. https://doi.org/10.5802/crmeca.74.
[30] Takezawa A, Kitamura M, Vtanabe SL, Silva ECN. Design methodology of piezoelectric energy-harvesting skin using topology optimization. Struct Multidiscip Optim 2014;49:281–97. https://doi.org/10.1007/s00158-013-0974-x.
[31] Naseer R, Abdelkefi A. Nonlinear modeling and efficacy of VIV-based energy harvesters: Monostable and bistable designs. Mech Syst Signal Process 2022;169:108775. https://doi.org/10.1016/j.ymssp.2021.108775.
[32] Yang K, Qiu T, Wang J, Tang L. Magnet-induced monostable nonlinearity for improving the VIV-galloping-coupled wind energy harvesting using combined cross-sectioned bluff body. Smart Mater Struct 2020;29:1–8. https://doi.org/10.1088/1361-665X/ab874c.
[33] Zhou Z, Qin W, Zhu P, Du W. Harvesting more energy from variable-speed wind by a multi-stable configuration with vortex-induced vibration and galloping. Energy 2021;237:121551. https://doi.org/10.1016/J.ENERGY.2021.121551.
[34] Qin W, Deng W, Pan J, Zhou Z, Du W, Zhu P. Harvesting wind energy with bi-stable snap-through excited by vortex-induced vibration and galloping. Energy 2019;189:116237. https://doi.org/10.1016/j.energy.2019.116237.
[35] Zou H-X, Li M, Zhao L-C, Gao Q-H, Wei K-X, Zuo L, et al. A magnetically coupled bistable piezoelectric harvester for underwater energy harvesting. Energy 2021;217:119429.
[36] Shan X, Sui G, Tian H, Min Z, Feng J, Xie T. Numerical analysis and experiments of an underwater magnetic nonlinear energy harvester based on vortex-induced vibration. Energy 2022;241:122933. https://doi.org/10.1016/j.energy.2021.122933.
[37] Xiao H, Wang X, John S. A dimensionless analysis of a 2DOF piezoelectric vibration energy harvester. Mech Syst Signal Process 2015;58:355–75. https://doi.org/10.1016/j.ymssp.2014.12.008.
[38] Blevins RD. Models for Vortex-Induced Vibration of Cylinders Based on Measured Forces. J Fluids Eng 2009:131. https://doi.org/10.1115/1.3222906.
[39] Vokoun D, Beleggia M, Heller L, Šittner P. Magnetostatic interactions and forces between cylindrical permanent magnets. J Magn Magn Mater 2009;321:3758–63. https://doi.org/10.1016/J.JMMM.2009.07.030.
[40] Muthalif AG, Hafizh M, Renno J, Paurobally MR. A hybrid piezoelectric-electromagnetic energy harvester from vortex-induced vibrations in fluid-flow; the influence of boundary condition in tuning the harvester. Energy Convers Manag 2022;256:115371. https://doi.org/10.1016/j.enconman.2022.115371.
[41] Norberg C. Fluctuating lift on a circular cylinder: Review and new measurements. J Fluids Struct 2003;17:57–96. https://doi.org/10.1016/S0889-9746(02)00099-3.
[42] Menter FR. Two-equation eddy-viscosity turbulence models for engineering applications. AIAA J 1994;32:1598–605. https://doi.org/10.2514/3.12149.
[43] Corbera Caraballo S, Olazagoitia Rodríguez JL, Lozano Ruiz JA, Álvarez FR. Optimization of a butterfly valve disc using 3D topology and genetic algorithms. Struct Multidiscip Optim 2017;56:941–57. https://doi.org/10.1007/s00158-017-1694-4.
[44] Kan J, Liao W, Wang S, Chen S, Huang X, Zhang Z. A piezoelectric wind energy harvester excited indirectly by a coupler via magnetic-field coupling. Energy Convers Manag 2021;240:114250. https://doi.org/10.1016/J.ENCONMAN.2021.114250.
[45] Trethewey MW. Window and overlap processing effects on power estimates from spectra. Mech Syst Signal Process 2000;14:267–78. https://doi.org/10.1006/mssp.1999.1274.
[46] Nguyen TQ, de Oliveira Correia JAF. Separation of the Structure Signal by the Maximal Overlap Discrete Wavelet Transform and Fast Fourier Transform. Adv Mater Sci Eng 2021;2021:1–15.
[47] Zhang LB, Abdelkefi A, Dai HL, Naseer R, Wang L. Design and experimental analysis of broadband energy harvesting from vortex-induced vibrations. J Sound Vib 2017;408:210–9. https://doi.org/10.1016/j.jsv.2017.07.029.